Energy Efficiency Optimization for RIS-Assisted UAV-Enabled MEC Systems

Xintong Qin *, Wenjuan Yu †, Zhengyu Song *, Tianwei Hou*, Yuanyuan Hao‡§, and Xin Sun *

* School of Electronic and Information Engineering, Beijing Jiaotong University, Beijing 100044, China
† School of Computing and Communications, InfoLab21, Lancaster University, Lancaster LA1 4WA, U.K.
‡ Institute of Telecommunication and Navigation Satellites, China Academy of Space Technology, Beijing 100094, China
§ Innovation Center of Satellite Communication System, China National Space Administration, Beijing 100094, China
Emails: {20111046, songzy, twhou, xsun}@bjtu.edu.cn, w.yu8@lancaster.ac.uk, yhao106@163.com

***Abstract*—The reconfigurable intelligent surface (RIS) can proactively modify the wireless communication environment and further improve the service quality of the wireless networks. Motivated by this vision, in this paper, we propose to introduce the RIS into the unmanned aerial vehicle (UAV) enabled mobile edge computing (MEC) systems. Considering both the amount of completed task bits and the energy consumption, the energy efficiency of the RIS-assisted UAV-enabled MEC systems is maximized by jointly optimizing the bit allocation, phase shift, and UAV trajectory via an iterative algorithm with a double-loop structure. Simulation results show that: 1) the UAV tends to fly closer to the RIS rather than the IoT devices; 2) the energy efficiency first increases and then decreases with the increase of the total amount of task-input bits of IoT devices; 3) higher energy efficiency can be achieved by our proposed algorithm.**

I. Introduction

In recent years, the number of Internet of Things (IoT) devices is dramatically increasing, which generates enormous volumes of data traffic and triggers higher demand for communication and computing capacities. Mobile edge computing (MEC) is recognized as an effective solution to tackle the computation-intensive and latency-critical tasks generated by these IoT devices [1]. However, the infrastructure-based MEC systems are difficult to provide MEC services for IoT devices located in remote areas. Fortunately, thanks to the inherent attributes such as flexible deployment, the unmanned aerial vehicle (UAV) can provide reliable computing services for IoT devices by equipping with an MEC server [2]–[5].

In order to further improve the offloading performance of IoT devices, an emerging technology called reconfigurable intelligent surface (RIS) has drawn great attentions and been introduced into the MEC systems recently. For instance, during a given mission period, the total amount of completed task-input bits is maximized in [6]–[8]. Simulation results demonstrate that the significant performance enhancement for MEC systems is able to be achieved with the aid of RIS. Aiming to minimize the energy consumption, the phase shift, transmit power, time and the decoding order are jointly optimized in [9]. Besides, the latency minimization and energy efficiency maximization problems in the RIS-assisted MEC are investigated in [10] and [11], respectively.

However, there are still few works focusing on the optimization of MEC systems assisted by both the UAV and RIS. The deployment of RIS to a certain extant facilitates the task offloading of IoT devices, but when a large amount of task bits is offloaded to the UAV-mounted MEC server, it will threaten the system's operating time considering the UAV's limited energy storage. Besides, although the UAV trajectory design has been intensively studied in UAV-assisted networks without RIS, the proposed algorithms cannot be directly applied to design the UAV trajectory with the participation of RIS. This is because the angle of departure (AoD) of the signal from the RIS to the UAV varies with the positions of UAV, which means the UAV trajectory design is coupled with the phase shift optimization.

Therefore, to bridge this research gap and tackle the aforementioned challenges, we investigate the RIS-assisted UAV-enabled MEC systems to maximize the energy efficiency, where the task bit allocation between IoT devices and MEC server, phase shift of RIS, and the UAV trajectory are jointly optimized. Simulation results verify that our proposed algorithm is able to achieve higher energy efficiency compared to the schemes with random phase, without trajectory optimization, without RIS, and the full offloading scheme.

II. System Model and Problem Formulation

A. System Model

We consider an RIS-assisted UAV-enabled MEC system, where an UAV mounted with an MEC server is employed to provide computing services for I IoT devices. An RIS with M reflection elements is installed on the surrounding building wall to assist IoT devices' task offloading. To ease of exposition, the IoT devices are denoted by $i \in \mathcal{I} \triangleq \{1, 2, ..., I\}$. The reflection elements of RIS are indexed by $m \in \mathcal{M} \triangleq \{1, 2, ..., M\}$.

The mission period T is discretized into N time slots and indexed by $n \in \mathcal{N} \triangleq \{1, 2, ..., N\}$. A 3D Cartesian coordinate system is adopted to describe the positions of UAV, RIS, and

978-1-6654-5975- 4/22/$31.00 ©

the IoT devices. Specifically, the horizontal position of the UAV at time slot n is represented as $\mathbf{q}[n] = (x_{\mathrm{U}}[n], y_{\mathrm{U}}[n])$. Similar to [1], the altitude of UAV is H, with $H > 0$. The horizontal position and the altitude of the first element on RIS are given by $\mathbf{w}_{\mathrm{R}} = (x_{\mathrm{R}}, y_{\mathrm{R}})$ and h_{R}, respectively. Besides, for the i-th IoT device, its altitude is zero and the horizontal position is $\mathbf{w}_i = (x_i, y_i)$.

1) Communication Model: Owing to the fact that the UAV flies at a high altitude, and the RIS is installed on the façade of a building, the communication link between the UAV and RIS can be assumed to be a line-of-sight (LoS) channel [12]. Thus, the channel gain between the UAV and the RIS at time slot n can be given by

$$\mathbf{h}_{\mathrm{R}}^{\mathrm{U}}[n] = \sqrt{\rho d_{\mathrm{RU}}^{-2}[n]} \left[1, ..., e^{-j\frac{2\pi}{\lambda}(M-1)d\varphi_{\mathrm{RU}}[n]}\right], \quad (1)$$

where ρ is the path loss at the reference $D_0 = 1$m; $d_{\mathrm{RU}}[n] = \sqrt{(H - h_{\mathrm{R}})^2 + \|\mathbf{q}[n] - \mathbf{w}_{\mathrm{R}}\|^2}$ denotes the distance between the UAV and the RIS at the n-th time slot; d is the antenna separation; λ is the carrier wavelength; $\varphi_{\mathrm{RU}}[n] = (x_{\mathrm{R}} - x_{\mathrm{U}}[n])/d_{\mathrm{RU}}[n]$ is the cosine of the AoD of the signal from the RIS to the UAV at time slot n.

The direct links from the IoT devices to the UAV are assumed to be blocked [2]. Thus, the channel gain from the i-th IoT device to the UAV at time slot n can be expressed as

$$h_i^{\mathrm{U}}[n] = \sqrt{\rho d_{i\mathrm{U}}^{-\varepsilon}[n]} g_{i\mathrm{U}}, \quad (2)$$

where $d_{i\mathrm{U}}[n] = \sqrt{\|\mathbf{q}[n] - \mathbf{w}_i\|^2 + H^2}$ is the distance between the UAV and the i-th IoT device at time slot n; ε is the path loss exponent and $g_{i\mathrm{U}}$ represents the random scattering component.

For the communication links from the IoT devices to the RIS, we assume that they are Rician fading channels [2], consisting of the LoS and non-LoS (NLoS) components. Hence, the channel gain between the i-th IoT device and the RIS at time slot n can be given by

$$\mathbf{h}_i^{\mathrm{R}}[n] = \sqrt{\rho d_{i\mathrm{R}}^{-\gamma}[n]} \left(\sqrt{\frac{\beta}{1+\beta}}\mathbf{h}_{i\mathrm{R}}^{\mathrm{LoS}} + \sqrt{\frac{1}{1+\beta}}\mathbf{h}_{i\mathrm{R}}^{\mathrm{NLoS}}\right), \quad (3)$$

where $d_{i\mathrm{R}} = \sqrt{\|\mathbf{w}_i - \mathbf{w}_{\mathrm{R}}\|^2 + {h_{\mathrm{R}}}^2}$ is the distance between the i-th IoT device and the RIS; γ denotes the path loss exponent; β represents the Rician factor; $\mathbf{h}_{i\mathrm{R}}^{\mathrm{LoS}}$ and $\mathbf{h}_{i\mathrm{R}}^{\mathrm{NLoS}}$ are the LoS component and NLoS component, respectively. For $\mathbf{h}_{i\mathrm{R}}^{\mathrm{LoS}}$, we have $\mathbf{h}_{i\mathrm{R}}^{\mathrm{LoS}}[n] = \left[1, e^{-j\frac{2\pi}{\lambda}d\varphi_{i\mathrm{R}}}, ..., e^{-j\frac{2\pi}{\lambda}(M-1)d\varphi_{i\mathrm{R}}}\right]^T$, where $\varphi_{i\mathrm{R}} = (x_i - x_{\mathrm{R}})/d_{i\mathrm{R}}$ is the cosine of the angle of arrival (AoA) of the signal from the i-th IoT device to the RIS.

Since the phase shift of each element of RIS can be dynamically adjusted by a controller, in this paper, the phase shift matrix of the RIS can be given by [13]

$$\mathbf{\Phi}[n] = \mathrm{diag}\left\{e^{j\theta_1[n]}, ..., e^{j\theta_M[n]}\right\}, \quad (4)$$

where $\theta_m[n] \in [0, 2\pi]$ is the phase shift of the m-th RIS element at the n-th time slot. Thus, the combined channel gain from the i-th IoT device to the UAV at time slot n can be expressed as

$$h_i[n] = h_i^{\mathrm{U}}[n] + (\mathbf{h}_i^{\mathrm{R}}[n])^H \mathbf{\Phi}[n]\mathbf{h}_{\mathrm{R}}^{\mathrm{U}}[n]. \quad (5)$$

Denote the bandwidth of the system as B. Benefiting from the partial offloading paradigm, the IoT devices can offload parts of their task-input data to the UAV. Besides, when the IoT devices offload tasks, the NOMA protocol is adopted to further improve the energy efficiency. To be specific, at each time slot, the IoT devices are ranked by the UAV in the ascending order of channel gain. Therefore, the order of the IoT devices for the UAV is denoted by $\Pi = \{\pi_1[n], \pi_2[n], ..., \pi_I[n]\}$, where $\pi_i[n]$ is the index of the IoT device with the i-th smallest channel gain to the UAV during time slot n.

After receiving the IoT device's signal, the UAV adopts the successive interference cancellation (SIC) technique to decode signals from multiple IoT devices. Specifically, when the UAV decodes the signal from IoT device $\pi_i[n]$, the signals from IoT device $\pi_1[n]$ to IoT device $\pi_{i-1}[n]$ are regarded as interference. Thus, the offloading data rate of IoT device $\pi_i[n]$ at the n-th time slot can be expressed as [3]

$$R_{\pi_i}^{\mathrm{off}}[n] = B\log\left(1 + \frac{p_{\pi_i}[n]|h_{\pi_i}[n]|^2}{\sum_{j=1}^{i-1} p_{\pi_j}[n]|h_{\pi_j}[n]|^2 + \sigma^2}\right), \quad (6)$$

where σ^2 is the noise power. $p_{\pi_i}[n]$ is the transmit power of IoT device $\pi_i[n]$, which is assumed to be predetermined in this paper. If the time slot index can be shown clearly in the variables, the order index $\pi_i[n]$ in the subscript is reduced to π_i for ease of exposition.

2) Computation Model: The task of each IoT device can be denoted by a positive tuple $\{L_i, C_i\}$, where L_i represents the minimal amount of task-input bits of IoT device i in the mission period. At each time slot, the IoT devices can simultaneously perform local computing and task offloading. Denote the amount of task bits that is computed by the UAV for IoT device i at time slot n as $l_i^{\mathrm{UAV}}[n]$. Since the UAV can only compute the task that has been offloaded and received, we have

$$R_i^{\mathrm{off}}[n]\, t \geq l_i^{\mathrm{UAV}}[n], \forall i \in \mathcal{I}, n \in \mathcal{N}. \quad (7)$$

In addition, to meet all IoT devices' minimum computation requirements, we have

$$\sum_{n=1}^{N} \left(l_i^{\mathrm{loc}}[n] + l_i^{\mathrm{UAV}}[n]\right) \geq L_i, \forall i \in \mathcal{I}. \quad (8)$$

where $l_i^{\mathrm{loc}}[n]$ is the task bits computed locally at IoT device i.

3) Energy consumption model: During time slot n, the task offloading energy consumption of IoT device i can be expressed as

$$E_i^{\mathrm{off}}[n] = p_i[n]t. \quad (9)$$

Then, based on [3], the local computing energy consumed

by IoT device i can be modeled as

$$E_i^{\mathrm{com}}[n] = \frac{\kappa_{\mathrm{IoT}}\left(l_i^{\mathrm{loc}}[n]\right)^3}{t^2}, \tag{10}$$

where κ_{IoT} is the effective capacitance coefficient.

With a similar model to the IoT device, the computing energy consumption of the UAV at time slot n is given by

$$E_{\mathrm{U}}^{\mathrm{com}}[n] = \sum_{i=1}^{I} \frac{\kappa_{\mathrm{UAV}}\left(l_i^{\mathrm{UAV}}[n]\right)^3}{t^2}, \tag{11}$$

where κ_{UAV} is the UAV's effective capacitance coefficient.

The flying energy consumption of the UAV is modeled as [14]

$$E_{\mathrm{U}}^{\mathrm{fly}}[n] = t\left(\tau_1 v^3[n] + \frac{\tau_2}{v[n]}\right), \tag{12}$$

where τ_1 and τ_2 are two parameters related to the UAVs' specifications.

B. Problem Formulation

In this paper, we aim to maximize the energy efficiency of the RIS-assisted UAV-enabled MEC system. At each time slot, the total amount of completed task bits are comprised of the offloading task bits and those computed locally at the IoT devices. Thus, at time slot n, the total amount of completed task bits of the system is

$$L[n] = \sum_{i=1}^{I}\left(l_i^{\mathrm{loc}}[n] + R_i^{\mathrm{off}}[n]\,t\right). \tag{13}$$

Meanwhile, the total energy consumption includes all IoT devices' energy consumption and the UAV's energy consumption, which can be given by

$$E[n] = \sum_{i=1}^{I}\left(E_i^{\mathrm{off}}[n] + E_i^{\mathrm{com}}[n]\right) + E_{\mathrm{U}}^{\mathrm{fly}}[n] + E_{\mathrm{U}}^{\mathrm{com}}[n] \tag{14}$$

Define the energy efficiency as the ratio of the total amount of completed task bits over the total energy consumption in the mission period [15]. Thus, the energy efficiency maximization problem for RIS-assisted UAV-enabled systems is formulated as

$$\max_{\mathbf{z}} \frac{\sum_{n=1}^{N} L[n]}{\sum_{n=1}^{N} E[n]} \tag{15a}$$

$$\text{s.t. } |\theta_m[n]| = 1, \forall m \in M, n \in N, \tag{15b}$$

$$\mathbf{q}[1] = \mathbf{q}_0, \mathbf{q}[N+1] = \mathbf{q}_F, \tag{15c}$$

$$||v[n]|| \le V_{\mathrm{Max}}, \forall n \in N, \tag{15d}$$

$$\frac{l_i^{\mathrm{loc}}[n] C_i}{t} \le F_i, \forall i \in \mathcal{I}, n \in \mathcal{N}, \tag{15e}$$

$$\frac{\sum_{i=1}^{I} l_i^{\mathrm{UAV}}[n]\, C_i}{t} \le F_{\mathrm{UAV}}, \forall n \in \mathcal{N}, \tag{15f}$$

$$(7), (8). \tag{15g}$$

where $\mathbf{z} = \left\{l_i^{\mathrm{loc}}[n], l_i^{\mathrm{UAV}}[n], \theta_m[n], \mathbf{q}[n]\right\}$. Constraint (15b) represents the feasible set of RIS's phase shift. Constraint (15c) is UAV's initial and final horizontal locations. Constraint (15d) represents that the speed of UAV must be less than the maximum speed. F_i and F_{UAV} are maximum CPU frequencies of IoT device i and the UAV, respectively. Constraints (15e) and (15f) mean that the workloads of IoT devices and UAV cannot exceed their maximum CPU frequencies.

III. Solution to the Formulated Problem

Due to the fractional structure of the objective function, and the closely coupled optimization variables in (15), it is difficult to obtain the globally optimal solution in polynomial time. To tackle these challenges, an iterative algorithm with a double-loop structure is proposed to maximize the energy efficiency and optimize the bit allocation $l_i^{\mathrm{loc}}[n]$ and $l_i^{\mathrm{UAV}}[n]$, phase shift of RIS $\theta_m[n]$, and the UAV trajectory $\mathbf{q}[n]$. In the outer loop, we exploit the Dinkelbach's method to handle the fraction programming and obtain the energy efficiency. With the given energy efficiency, the coupled variables are iteratively optimized in the inner loop.

Firstly, we equivalently transform problem (15) as the following parametric problem:

$$\begin{aligned} &\max_{\mathbf{z},\alpha} \sum_{n=1}^{N} L[n] - \alpha \sum_{n=1}^{N} E[n], \\ &\text{s.t.} (15\text{b}) - (15\text{g}), \end{aligned} \tag{16}$$

where α is the introduced auxiliary parameter. According to the Dinkelbach's method, the optimal solution $\mathbf{z}^*$ of problem (15) can be obtained when $\max_{\mathbf{z}} \left(\sum_{n=1}^{N} L[n] - \alpha^* \sum_{n=1}^{N} E[n]\right) = 0$, where α^* is the optimal objective value of problem (15). However, the optimal α^* cannot be obtained in advance. Hence we propose an iterative algorithm to update α. The details can be seen in Algorithm 1.

In Algorithm 1, problem (16) needs to be solved with given $\alpha^{(k)}$. However, with given energy efficiency $\alpha^{(k)}$, problem (16) is still non-convex due to the coupling among optimization variables. Therefore, we decompose problem (16) into three subproblems by adopting the BCD technique, namely, bit allocation, phase shift optimization, and UAV trajectory optimization. And then an iterative algorithm is proposed to solve them in an alternating manner.

A. Bit Allocation Among IoT devices and the UAV

With given $\theta_m[n]$ and $\mathbf{q}[n]$, the bit allocation problem is reformulated from (16) as

$$\max_{l_i^{\mathrm{loc}}[n], l_i^{\mathrm{UAV}}[n]} \sum_{n=1}^{N} L[n] - \alpha \sum_{n=1}^{N} E[n] \tag{17a}$$

$$\text{s.t.} (15\text{e}) - (15\text{g}). \tag{17b}$$

Note that problem (17) is a standard convex optimization problem, and can be readily solved via CVX.

Algorithm 1 Dinkelbach's algorithm for maximizing the energy efficiency

1. Initialize $\mathbf{z}$, iterative number $k=1$.
2. **repeat**:
3. Solve problem (16) for given $\alpha^{(k)}$, and obtain the optimal solution $\mathbf{z}^{(k)}$.
4. Calculate $F(\alpha^{(k)})=\left|\sum_{n=1}^{N}L[n]-\alpha\sum_{n=1}^{N}E[n]\right|^{(k)}$.
5. **if** $F(\alpha^{(k)})\leq\delta$ then
6. $\alpha^{*}=\frac{\sum_{n=1}^{N}L[n]^{(k)}}{\sum_{n=1}^{N}E[n]^{(k)}}$; $\mathbf{z}^{*}=\mathbf{z}^{(k)}$; break.
7. **else** $\alpha^{(k+1)}=\frac{\sum_{n=1}^{N}L[n]^{(k)}}{\sum_{n=1}^{N}E[n]^{(k)}}$; $k=k+1$.
8. **Until** $k\geq N_{\max}$.
9. **Output**: the optimal energy efficiency α^{*} and the corresponding solution $\mathbf{z}^{*}$.

B. Phase Shift Optimization for RIS

For given $l_i^{\mathrm{loc}}[n]$, $l_i^{\mathrm{UAV}}[n]$, and $\mathbf{q}[n]$, problem (16) can be reformulated as

$$\begin{aligned}&\max_{\theta_m[n]}\sum_{n=1}^{N}\sum_{i=1}^{I}BtR_{\pi_i}^{\mathrm{off}}[n],\\&\text{s.t.}\,|\theta_m[n]|=1,\forall m\in M,n\in N.\end{aligned}\tag{18}$$

To solve problem (37), we first define $\mathbf{h}_{\pi_i}^{\mathrm{RIS}}[n]=\mathbf{h}_{\pi_i}^{\mathrm{R}}[n]^{H}\mathrm{diag}\left(\mathbf{h}_{\mathrm{R}}^{\mathrm{U}}[n]\right)$. Then, the channel gain between IoT device $\pi_i[n]$ and the UAV can be expressed as

$$\begin{aligned}|h_{\pi_i}[n]|^2&=\left|h_{\pi_i}^{\mathrm{U}}[n]+(\mathbf{h}_{\pi_i}^{\mathrm{R}}[n])^{H}\mathrm{diag}(\mathbf{\Phi}[n])\mathbf{h}_{\mathrm{R}}^{\mathrm{U}}[n]\right|^2\\&=\mathrm{Tr}\left(\mathbf{H}_{\pi_i}[\mathrm{n}]\mathbf{\Theta}[n]\right)+\left(h_{\pi_i}^{\mathrm{U}}[n]\right)^2,\end{aligned}\tag{19}$$

where $\mathbf{H}_{\pi_i}[n]=\begin{pmatrix}\mathbf{h}_{\pi_i}^{\mathrm{RIS}}[n]^{H}\mathbf{h}_{\pi_i}^{\mathrm{RIS}}[n] & \mathbf{h}_{\pi_i}^{\mathrm{RIS}}[n]^{H}\mathbf{h}_{\pi_i}^{\mathrm{U}}[n]\\ \mathbf{h}_{\pi_i}^{\mathrm{U}}[n]\mathbf{h}_{\pi_i}^{\mathrm{RIS}}[n] & 0\end{pmatrix}$, and $\mathbf{\Theta}[n]=\bar{\mathbf{\Phi}}[n]\left(\bar{\mathbf{\Phi}}[n]\right)^{H}$ is a positive semidefinite matrix with $\bar{\mathbf{\Phi}}[n]=[e^{j\theta_1[n]},...,e^{j\theta_M[n]},x]^{T}$. x is an auxiliary scalar. By substituting (19) into problem (18), we have

$$\begin{aligned}R_{\pi_i}^{\mathrm{off}}[n]=&\log_2\left(\sum_{j=1}^{i}p_{\pi_j}[n](\mathrm{Tr}(\mathbf{H}_{\pi_j}[\mathrm{n}]\mathbf{\Theta}[n])+(h_{\pi_j}^{\mathrm{U}}[n])^2)+\sigma^2\right)\\&-\log_2\left(\sum_{j=1}^{i-1}p_{\pi_j}[n]\left(\mathrm{Tr}(\mathbf{H}_{\pi_j}[\mathrm{n}]\mathbf{\Theta}[n])+\left(h_{\pi_j}^{\mathrm{U}}[n]\right)^2\right)+\sigma^2\right)\\&=W_1^i[n]-W_2^i[n]\end{aligned}\tag{20}$$

Thus, problem (18) can be transformed into

$$\max_{\mathbf{\Theta}[n]}\sum_{n=1}^{N}\sum_{i=1}^{I}\left(W_1^i[n]-W_2^i[n]\right)\tag{21a}$$

$$\text{s.t.}\,\Theta_{m,m}[n]=1,\forall m\in\mathcal{M},n\in\mathcal{N},\tag{21b}$$

$$\mathrm{rank}(\mathbf{\Theta}[n])=1,\forall n\in\mathcal{N}.\tag{21c}$$

We find the objective function of (21) is the difference of concave functions, which can be handled by exploiting the DC programming technique [8]. Thus, the second term of the objective function can be approximated as

$$\begin{aligned}W_2^i[n]\leq&\frac{\sum_{j=1}^{i-1}p_{\pi_j}[n]\left\langle\left(\mathbf{\Theta}[n]-\mathbf{\Theta}[n]^{(l)}\right),\nabla_{\mathbf{\Theta}}\mathrm{Tr}\left(\mathbf{H}_{\pi_j}[n]\mathbf{\Theta}[n]\right)\big|_{\mathbf{\Theta}=\mathbf{\Theta}^{(l)}}\right\rangle}{\ln 2\left(\sum_{j=1}^{i-1}p_{\pi_j}[n]\left(\mathrm{Tr}\left(\mathbf{H}_{\pi_j}[n]\mathbf{\Theta}[n]^{(l)}\right)+\left|h_{\pi_j}^{D}[n]\right|^2\right)+\sigma^2\right)}\\&+(W_2^i[n])^{(l)}=\tilde{W}_2^i[n]\end{aligned}\tag{22}$$

For constraint (21c), we exploit the semi-definite programming relaxation (SDR) technique such that problem (21) can be expressed as [16]

$$\max_{\mathbf{\Theta}[n]}\sum_{n=1}^{N}\sum_{i=1}^{I}\left(W_1^i[n]-\tilde{W}_2^i[n]\right)\tag{23a}$$

$$\text{s.t.}\,\mathbf{\Theta}_{m,m}[n]=1,\forall m\in\mathcal{M},n\in\mathcal{N},\tag{23b}$$

$$\mathbf{\Theta}[n]\succ 0,\forall n\in\mathcal{N},\tag{23c}$$

Note that problem (23) is a standard convex semi-definite programming and can be handled via classic convex toolboxes, such as the SDP solver in the CVX tool [17]. Then, we iteratively update $\mathbf{\Theta}[n]$ by solving problem (23) until convergence. During the iteration, when the rank of $\mathbf{\Theta}[n]$ is larger than one, the Gaussian randomization method is adopted to recover $\mathbf{\Phi}[n]$ from $\mathbf{\Theta}[n]$.

C. UAV Trajectory Optimization

Finally, supposing $l_i^{\mathrm{loc}}[n]$ and $l_i^{\mathrm{UAV}}[n]$, as well as $\theta_m[n]$ are given, problem (16) can be reformulated as

$$\begin{aligned}&\max_{\mathbf{q}[n]}\sum_{n=1}^{N}\sum_{i=1}^{I}BtR_{\pi_i}^{\mathrm{off}}[n]-t\alpha\sum_{n=1}^{N}\left(\tau_1 v^3[n]+\tfrac{\tau_2}{v[n]}\right)\\&\text{s.t.}(7),(15\mathrm{c}),(15\mathrm{d}).\end{aligned}\tag{24}$$

Due to constraint (7) and the objective function, problem (24) is also non-convex and difficult to solve. Therefore, we firstly define $M_1^i[n]=B\log\left(\sum_{j=1}^{i}p_{\pi_j}[n]\left|h_{\pi_j}[n]\right|^2+\sigma^2\right)$ and $M_2^i[n]=B\log\left(\sum_{j=1}^{i-1}p_{\pi_j}[n]\left|h_{\pi_j}[n]\right|^2+\sigma^2\right)$. The offloading rate of IoT device $\pi_i[n]$ at time slot n can be given by $R_{\pi_i}^{\mathrm{off}}[n]=M_1^i[n]-M_2^i[n]$. With optimal phase shift $\theta_m[n]$, the channel gain between IoT device $\pi_i[n]$ and the UAV can be expressed as [18]

$$\begin{aligned}h_{\pi_i}[n]&=h_{\pi_i}^{\mathrm{U}}[n]+(\mathbf{h}_{\pi_i}^{\mathrm{R}}[n])^{H}\mathbf{\Phi}[n]\mathbf{h}_{\mathrm{R}}^{\mathrm{U}}[n]\\&=\frac{\sqrt{\rho}|g_{\pi_i\mathrm{U}}|}{d_{\pi_i\mathrm{U}}^{\varepsilon/2}[n]}+\frac{\sqrt{\rho}\sum_{m=1}^{M}|h_{\pi_i\mathrm{R},m}|}{d_{\mathrm{RU}}[n]}.\end{aligned}\tag{25}$$

Then, the auxiliary variables $u_{\pi_i}[n]$ and $w[n]$ are introduced with $d_{\pi_i\mathrm{U}}[n]\leq u_{\pi_i}[n],d_{\mathrm{RU}}[n]\leq w[n]$. By replacing the term $d_{\pi_i\mathrm{U}}[n]$ and $d_{\mathrm{RU}}[n]$ in $M_1^i[n]$ with $u_{\pi_i}[n]$ and $w[n]$, we can obtain

$$\tilde{M}_1^i[n]=B\log\left(\sum_{j=1}^{i}p_{\pi_i}[n]\,\Xi(u_{\pi_i}[n],w[n])^2+\sigma^2\right),\tag{26}$$

TABLE I: Simulation Parameters [6] [14]

Parameters	Values	Parameters	Values
B	30 MHz	θ_1, θ_2	0.00614, 15.976
$V_{\max}$	10 m/s	β_0	-30 dB
N	20	σ^2	-50 dBm
H	40 m	h_R	20 m
F_i	3 GHz	F_{UAV}	12 GHz
γ	2.8	ε	3.5

where $\Xi\left(u_{\pi_i}[n], w[n]\right) = \frac{\sqrt{\rho}\left|g_{\pi_i \text{U}}\right|}{u_{\pi_i \text{U}}^{\varepsilon/2}[n]} + \frac{\sqrt{\rho}\sum_{m=1}^{M}\left|h_{\pi_i \text{R},m}\right|}{w[n]}$. Similarly, for $M_2^i[n]$, we have

$$\tilde{M}_2^i[n] = B\log\left(\sum_{j=1}^{i-1} p_{\pi_i}[n]\,\Xi(u_{\pi_i}[n], w[n])^2 + \sigma^2\right). \quad (27)$$

In addition, for the term $v[n]$ in the denominator, $\bar{v}[n]$ is introduced with $\bar{v}[n] \leq v[n]$. Then, a lower-bound of $\tilde{M}_1^i[n]$ can be expressed as

$$\begin{aligned}\tilde{M}_1^i[n] \geq \hat{M}_1^i[n] = &\log A_i[n] + \tfrac{B_i[n]}{A_i[n]\ln 2}\left(u_{\pi_i}[n] - u_{\pi_i}[n]^{(l)}\right) \\ &+ \tfrac{C_i[n]}{A_i[n]\ln 2}\left(w[n] - w[n]^l\right),\end{aligned} \quad (28)$$

where $A_i[n] = \sum_{j=1}^{i} p_{\pi_j}[n]\Xi\left(u_{\pi_j}[n]^{(l)}, w[n]^{(l)}\right)^2 + \sigma^2$, $C_i[n] = -p_{\pi_i}[n]\Xi\left(u_{\pi_i}[n]^{(l)}, w[n]^{(l)}\right)\frac{\sqrt{\rho}\sum_{m=1}^{M}\left|h_{\pi_i R,m}\right|}{w^2[n]}$, and $B_i[n] = -p_{\pi_i}[n]\Xi\left(u_{\pi_i}[n]^{(l)}, w[n]^{(l)}\right)\frac{\varepsilon\sqrt{\rho}\left|g_{\pi_i U}\right|}{u_{\pi_i}^{\varepsilon/2+1}[n]}$.

Similarly, constraints (47b)-(47d) can be approximated as

$$(d_{\pi_i U}[n])^2 + (u_{\pi_i}[n]^{(l)})^2 - 2u_{\pi_i}[n]^{(l)}u_{\pi_i}[n] \leq 0, \quad (29)$$

$$(d_{RU}[n])^2 + (w[n]^{(l)})^2 - 2w[n]^{(l)}w[n] \leq 0, \quad (30)$$

$$\begin{aligned}&\bar{v}[n]^2 t^2 + \left\|\mathbf{q}[n]^{(l)} - \mathbf{q}[n-1]^{(l)}\right\|^2 \\ &-2\left(\mathbf{q}[n]^{(l)} - \mathbf{q}[n-1]^{(l)}\right)^T\left(\mathbf{q}[n] - \mathbf{q}[n-1]\right) \leq 0.\end{aligned} \quad (31)$$

Then, problem (24) can be reformulated as a convex optimization problem, and can be solved efficiently by CVX [19]. The auxiliary variables $u_{\pi_i}[n], w[n], \bar{v}[n]$ and $\mathbf{q}[n]$ are iteratively updated until convergence. Finally, problem (24) is effectively solved and the optimized UAV trajectory can be obtained.

Based on the obtained solutions to the three subproblems, the proposed BCD algorithm for solving problem (16) with given energy efficiency is summarized in Algorithm 2. Therefore, according to Algorithm 1, the original problem (15) is able to be effectively tackled by iteratively updating the energy efficiency in the outer-loop and jointly optimizing $l_i^{\text{loc}}[n]$ and $l_i^{\text{UAV}}[n]$, $\theta_m[n]$, and $\mathbf{q}[n]$ in the inner-loop via Algorithm 2.

Algorithm 2 BCD algorithm for solving Problem (16)

1. Initialize α_k, iterative number $l = 1$.
2. **repeat**:
3. Solve problem (17) to obtain $l_i^{\text{loc}}[n]^{(l)}$ and $l_i^{\text{UAV}}[n]^{(l)}$ for given $\theta_m[n]$ and $\mathbf{q}[n]$.
4. Solve problem (18) to obtain $\theta_m[n]^{(l)}$ according to the updated $l_i^{\text{loc}}[n]^{(l)}$, $l_i^{\text{UAV}}[n]^{(l)}$ and given $\mathbf{q}[n]$.
5. Solve problem (23) to obtain $\mathbf{q}[n]^{(l)}$ with updated $l_i^{\text{loc}}[n]^{(l)}$, $l_i^{\text{UAV}}[n]^{(l)}$, and $\theta_m[n]^{(l)}$.
6. Calculate $F\left(\mathbf{z}^{(l)}\right) = \left|\sum_{n=1}^{N} L[n] - \alpha_k \sum_{n=1}^{N} E[n]\right|$.
7. Update the iterative index $l = l + 1$.
8. **Until**: $l > N_{\max}$ or $\left|F(\mathbf{z}^{(l+1)}) - F(\mathbf{z}^{(l)})\right| \leq \delta$.
9. **Output**: bit allocation $l_i^{\text{loc}}[n]^*$ and $l_i^{\text{UAV}}[n]^*$, phase shift $\theta_m[n]^*$, and UAV trajectory $\mathbf{q}[n]^*$.

IV. Simulation Results

In this section, we present simulation results and compare the proposed energy efficiency maximization algorithm with other baselines. In the simulations, there are 6 IoT devices and they have the same amount of task-input bits, i.e., $L_1 = L_2 = ... = L_I$. The rest of simulation parameters is summarized in Table I.

Fig. 1(a) demonstrates the convergence behaviours of the proposed energy efficiency maximization algorithm in the RIS-assisted UAV-enabled MEC system with $T = 10$ sec. We observe that the energy efficiency is increased rapidly at first and converges after around 5-6 iterations. Moreover, under different numbers of RIS elements, the proposed algorithm still converges fast.

Fig. 1(b) illustrates the trajectory of UAV under two different scenarios. Under the scheme without RIS, it can be observed that the UAV tends to fly closer to the IoT devices in order to achieve higher channel gains. On the contrary, in our proposed RIS-assisted UAV-enabled MEC system, we observe that the UAV tends to fly closer to the RIS. The reasons behind that can be explained as follows. When the RIS is deployed to help IoT devices' task offloading, there is a compromise for the UAV between the direct links and the reflecting links. By exploiting our proposed algorithm to reconfiguring the phase shift of RIS, the reflected signals is able to be combined constructively to greatly enhance the UAV's received signal power. Therefore, the UAV tends to fly closer to the RIS rather than the IoT devices in order to fully utilize the channel gains brought by the RIS and increase the energy efficiency.

Fig. 1(c) shows the energy efficiency versus the total amount of task-input bits of IoT devices. With the deployment of RIS, we observe that our proposed algorithm can achieve a higher energy efficiency than the other schemes, since the bit allocation, phase shift, and UAV trajectory are jointly optimized. Moreover, because the increase rate of exponential function is faster than the linear function, it can be seen that besides the full offloading scheme, the energy efficiency of all schemes first increases and then decreases. While for the full offloading scheme, the energy efficiency only shows a decrease trend since the amount of offloading bits of IoT devices in the full offloading scheme is greatly larger than the other schemes. Besides, it can also be observed that if the phase shifts are

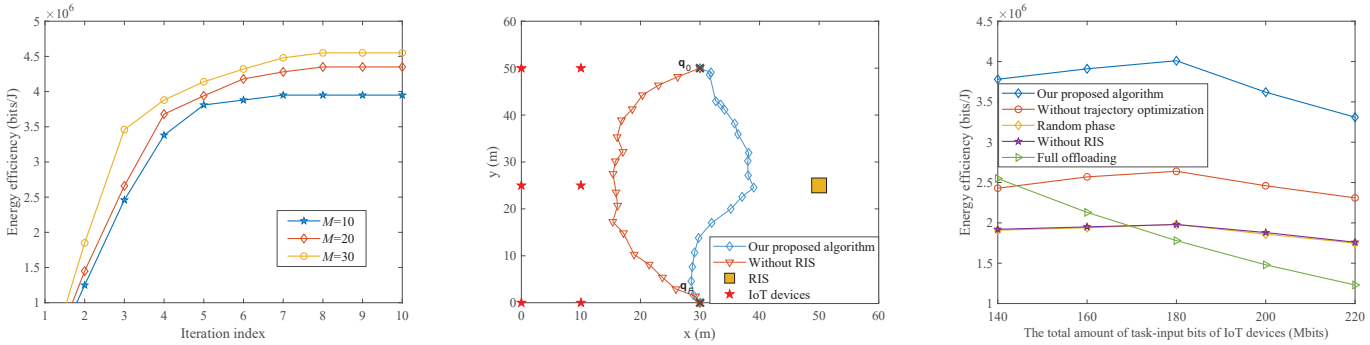

(a) (b) (c)

Fig. 1. (a) Energy efficiency versus the iteration index. (b) UAV trajectories under two different scenarios. (c) Energy efficiency versus the amount of task-input bits of IoT devices.

randomly chosen, the performance gain brought by the RIS over the scheme without RIS is negligible. This is because for the random phase scheme, the channel gain of the reflecting link is nearly equal to zero when those reflected signals via RIS are combined at the UAV. This result demonstrates the significance of phase shift optimization in our proposed system.

V. Conclusion

In this paper, the RIS-assisted UAV-enabled MEC systems were investigated with the aim to maximize the energy efficiency, where an iterative algorithm with a double-loop structure was proposed to jointly optimize the bit allocation, phase shift, and UAV trajectory. Simulation results have shown that our proposed algorithm outperformed other baselines. It was also observed that with the aid of RIS, the energy efficiency can be greatly improved only when the phase shift was carefully designed, and the UAV tended to fly closer to the RIS to obtain a better channel condition, which was quite different from the UAV-enabled MEC without RIS.

Acknowledgement

This work was supported by the National Natural Science Foundation of China under Grant 61901027.

References

[1] J. Ji, K. Zhu, C. Yi, and D. Niyato, "Energy consumption minimization in UAV-assisted mobile-edge computing systems: Joint resource allocation and trajectory design," *IEEE Internet of Things Journal*, vol. 8, no. 10, pp. 8570–8584, May 2021.

[2] H. Mei, K. Yang *et al.*, "Joint trajectory-task-cache optimization with phase-shift design of RIS-assisted UAV for MEC," *IEEE Wireless Communications Letters*, vol. 10, no. 7, pp. 1586–1590, Jul. 2021.

[3] X. Zhang, J. Zhang, J. Xiong, L. Zhou, and J. Wei, "Energy-efficient multi-UAV-enabled multiaccess edge computing incorporating NOMA," *IEEE Internet Things J.*, vol. 7, no. 6, pp. 5613–5627, Jun. 2020.

[4] Z. Yang, C. Pan, K. Wang, and M. Shikh-Bahaei, "Energy efficient resource allocation in UAV-enabled mobile edge computing networks," *IEEE Trans. Wirel. Commun.*, vol. 18, no. 9, pp. 4576–4589, Sep. 2019.

[5] Z. Song, X. Qin, Y. Hao *et al.*, "A comprehensive survey on aerial mobile edge computing: Challenges, state-of-the-art, and future directions," *Computer Communications*, vol. 191, pp. 233–256, Jul. 2022.

[6] S. Mao, N. Zhang *et al.*, "Computation rate maximization for intelligent reflecting surface enhanced wireless powered mobile edge computing networks," *IEEE Trans. Veh. Technol.*, vol. 70, no. 10, pp. 10 820–10 831, Oct. 2021.

[7] Z. Chu, P. Xiao *et al.*, "Intelligent reflecting surface assisted mobile edge computing for internet of things," *IEEE Wireless Communications Letters*, vol. 10, no. 3, pp. 619–623, Mar. 2021.

[8] X. Hu, C. Masouros, and K.-K. Wong, "Reconfigurable intelligent surface aided mobile edge computing: From optimization-based to location-only learning-based solutions," *IEEE Transactions on Communications*, vol. 69, no. 6, pp. 3709–3725, Jun. 2021.

[9] Z. Li, M. Chen, Z. Yang, J. Zhao, Y. Wang, J. Shi, and C. Huang, "Energy efficient reconfigurable intelligent surface enabled mobile edge computing networks with NOMA," *IEEE Transactions on Cognitive Communications and Networking*, vol. 7, no. 2, pp. 427–440, Jun. 2021.

[10] T. Bai, C. Pan, Y. Deng, M. Elkashlan, A. Nallanathan, and L. Hanzo, "Latency minimization for intelligent reflecting surface aided mobile edge computing," *IEEE Journal on Selected Areas in Communications*, vol. 38, no. 11, pp. 2666–2682, Nov. 2020.

[11] C. Huang, A. Zappone, G. C. Alexandropoulos, M. Debbah, and C. Yuen, "Reconfigurable intelligent surfaces for energy efficiency in wireless communication," *IEEE Transactions on Wireless Communications*, vol. 18, no. 8, pp. 4157–4170, Aug. 2019.

[12] X. Liu, Y. Liu, and Y. Chen, "Machine learning empowered trajectory and passive beamforming design in UAV-RIS wireless networks," *IEEE J. Sel. Areas Commun.*, vol. 39, no. 7, pp. 2042–2055, Jul. 2021.

[13] Y. Liu, X. Liu, X. Mu, T. Hou, J. Xu, M. Di Renzo, and N. Al-Dhahir, "Reconfigurable intelligent surfaces: Principles and opportunities," *IEEE Commun. Surveys Tuts.*, vol. 23, no. 3, pp. 1546–1577, 3rd Quarter 2021.

[14] X. Hu, K.-K. Wong, and Y. Zhang, "Wireless-powered edge computing with cooperative UAV: Task, time scheduling and trajectory design," *IEEE Transactions on Wireless Communications*, vol. 19, no. 12, pp. 8083–8098, Dec. 2020.

[15] J. Zhang *et al.*, "Computation-efficient offloading and trajectory scheduling for multi-UAV assisted mobile edge computing," *IEEE Trans. Veh. Technol.*, vol. 69, no. 2, pp. 2114–2125, Feb. 2020.

[16] Q. Wu and R. Zhang, "Intelligent reflecting surface enhanced wireless network via joint active and passive beamforming," *IEEE Transactions on Wireless Communications*, vol. 18, no. 11, pp. 5394–5409, Nov. 2019.

[17] C. Wu, X. Mu, Y. Liu, X. Gu, and X. Wang, "Resource allocation in STAR-RIS-aided networks: OMA and NOMA," *IEEE Transactions on Wireless Communications*, vol. 21, no. 9, pp. 7653–7667, Sep. 2022.

[18] S. Li, B. Duo, X. Yuan, Y.-C. Liang, and M. Di Renzo, "Reconfigurable intelligent surface assisted UAV communication: Joint trajectory design and passive beamforming," *IEEE Wireless Communications Letters*, vol. 9, no. 5, pp. 716–720, May 2020.

[19] T. Zhang, Y. Xu, J. Loo, D. Yang, and L. Xiao, "Joint computation and communication design for UAV-assisted mobile edge computing in IoT," *IEEE Trans. Ind. Inform.*, vol. 16, no. 8, pp. 5505–5516, Aug. 2020.